25

Electromechanical 3D Optoelectronic Scanners: Resolution Constraints and Possible Ways of Improvement

Oleg Sergiyenko[1], Vera Tyrsa[2], Luís C. Basaca-Preciado[1], Julio C. Rodríguez-Quiñones[1], Wilmar Hernández[4], Juan I. Nieto-Hipólito[1], Moisés Rivas Lopez[1] and Oleg Starostenko[3]
[1]Autonomous University of Baja California, Mexicali-Ensenada,
[2]Polytechnic University of Baja California, Mexicali,
[3]Universidad de Las Americas, Puebla,
[4]Polytechnic University of Madrid,
[1,2,3]Mexico
[4]Spain

1. Introduction

Non-Contact optoelectronic 3D measurement is a rapidly growing field. Three-Dimensional Non-Contact Measurement Technologies are very common for research due to multiple practical applications expecting for its benefits. Many fields are using in any way 3D measurements or shape recognition, some of them there are vision assisted assembly in various branches of industry, autonomous mobile robots navigation, structural health monitoring, micro surfaces inspections, precise automated surgery, etc.

In this chapter it is expedient to mention and briefly cross-compare the following emerging technologies for 3D measurements: laser scanners, lasers based on conoscopy holography technology and 3D cameras.

Laser scanners: Most contemporary non-contact 3D measurement devices are based on laser range scanning. The simplest devices (Fischer, 2007) are based on the laser triangulation technique. This is an active stereoscopic technique in which the distance of the object is computed by means of a directional light source and a video camera. The CCD camera's 2D array captures the image of surface profile and digitizes all data points along the laser disadvantage of this method is that a single camera collects only a small percentage of the reflected energy. The amount of the collected energy can be drastically increased by trapping the entire reflection cone, thus significantly increasing the precision and reliability of the measurements.

Lasers based on Conoscopic Holography technology: Conoscopic Holography is a simple implementation of a particular type of polarized light interference process based on crystal optics. In the basic interference set-up, a point of light is projected onto a diffuse object. This point creates a light point, which diffuses light in every direction. In a conoscopic system, a complete solid angle of the diffused light is analyzed by the system. The measurement

process retrieves the distance of the light point from a fixed reference plane. The problem inherent in laser scanning is its relatively low measurement speed, though it is faster than traditional contact Coordinate measurements machines (CMM's).

a) b)

Fig. 1. A scanner laser (a) and a 3D camera (b)

3D cameras**:** 3D photography is based on reconstructing 3D data from 2D images, taken from different points of view (stereo- graphic) the basic problem with this approach is the correspondence problem. In 3D cameras a pattern is projected on the object and the same pattern points are identified on each image. This approach is much more efficient, since it does not require marking specific points, and it can produce a very large number of measurements in one shot of camera.

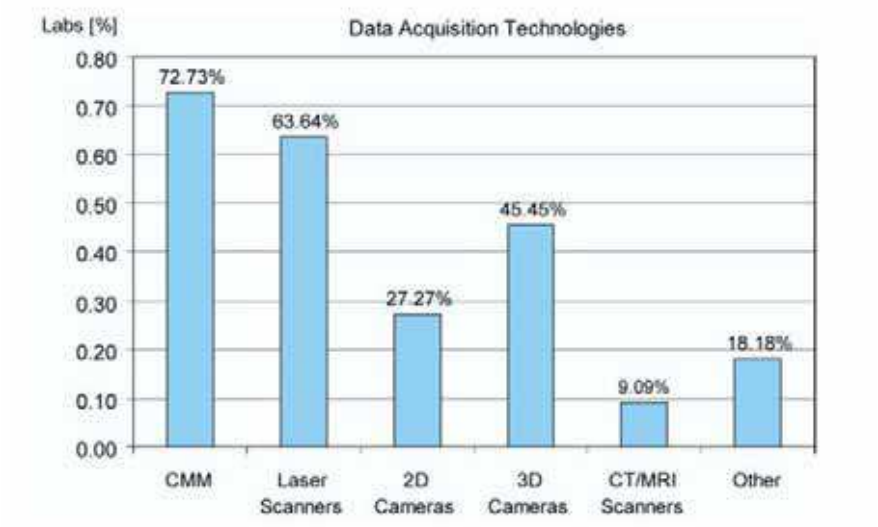

Fig. 2. Distribution of 3D scanning technologies among 23 engineering universities and research centers across Europe according to (Fischer, 2007)

The typical distribution of 3D scanning technologies research among engineering universities and research centers is given on Fig.2. CMM is still numerous due to non-innovative routines in industry with traditional investments for research. But this technology is contact and applicable for very limited area of tasks. So, the future is for laser scanning and 3D camera vision.
In fact, specialists already get a consensus regard to most evidences of these two branches. Cameras are winning in a point of less energy consuming and a relatively longer range of action. But laser scanning systems always win at resolution, accuracy and data processing time.
Basing in this, it is easy to show that for various tasks (such as: vision assisted assembly, robot navigation in densely cluttered environment, structural health monitoring, etc.) the laser scanner is an optimal way to obtain quality 3D information about objects in nearest surrounding in higher resolution.
But the majority of modern laser scanners have a certain part of rotating/moving electromechanical components, which are closely related with such negative phenomenon like mechanical vibrations, friction and wear, mechanical delays, etc.
Present paper scope is precisely to research what are the most prospective ways to increase the electromechanical laser scanners resolution and robustness. With this aim let us deeper study most typical approaches to laser scanner construction, as one of the most promising technical vision system (TVS).

2. Typical laser scanner constructions and their constraints

According to the recent literature electromechanical laser scanners have sufficiently variety in its constructions. At the same time, they have enough similarities and common components in its general structure. Let will see some of the typical constructions of electromechanical laser scanners for to have the possibility systemize such constructions and define their common advantages and lacks.
An obvious optimization of the measurement system (Wulf & Wagner, 2003) is to take the scanning method that is most suitable for the application. However, taking a 2D laser scanner with 180° scanning range and a servo drive it results in a number of possible combinations of scan planes and rotation axis to get a 3D scan. This section describes four of these combinations. We have named the scanning methods as *pitching scan*, *rolling scan*, *yawing scan* and *yawing scan top*. The *pitching scan* (Fig. 3a) has a horizontal scan plane and is pitching up and down. This method is for example used in (Surmann et al., 2001) and (Hähnel & Burgard, 2002). A method that is newly introduced here is the *rolling scan* (Fig. 3b). This scan is rotating around the center of the scanner, with the advantage of only one focus point in front of the sensor. The *yawing scan* (Fig. 3c) and the *yawing scan top* (Fig. 3d) has a vertical scan plane and is rotating around the upright z-axis. This method is used e.g. by (Wulf, O. & Wagner, B. (2003).
Let us compare constructions and advantages/disadvantages of the different laser scanner constructions according to the next literature sources: (Son et al., 2002), (Wulf & Wagner, 2003), (Nüchter, 2007), (Nüchter, 2008), (Wulf et al., 2004), (Surmann, 2003), (Surmann et al., 2001), (Hähnel & Burgard, 2002), (Blais et al., 1988), (Blais et al., 2000), (Beraldin et al., 2000), (Andersen et al., 2006), (Laurin et al., 1996), (Blais et al., 1991), (Klöör et al., 1993), (Vandapel et al., 2004), (Montemerlo & Thrun, 2004), (Pagnottelli et al., 2005), (Sergiyenko et al., 2006).

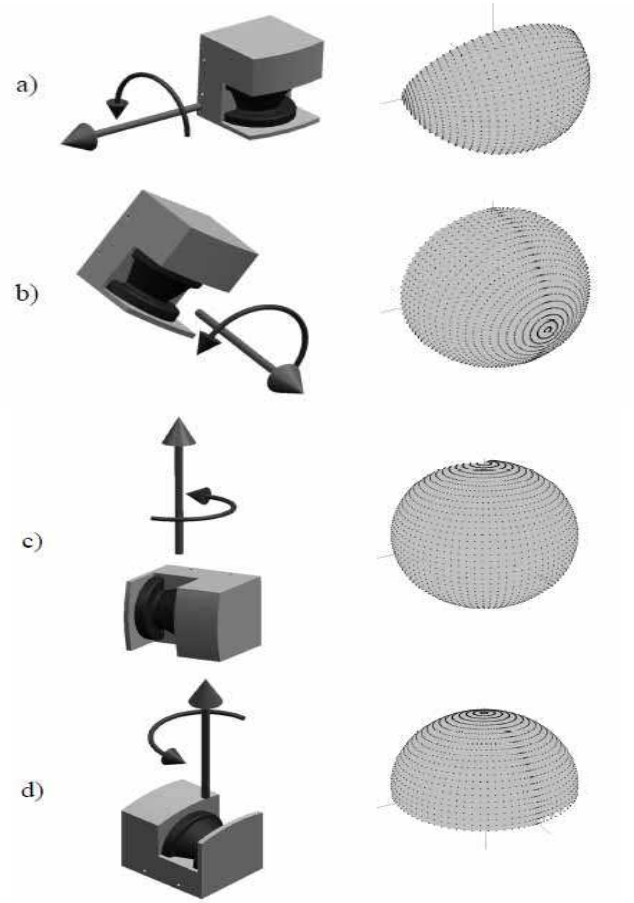

Fig. 3. The *pitching scan* (a), the *rolling scan* (b), the *yawing scan* (c) and the *yawing scan top* (d) (Wulf & Wagner, 2003)

2.1 Automated laser scanning system for reverse engineering and inspection

The mechanism of the 3D laser scanner used in this research (Son et al., 2002) is illustrated in Fig. 4. A laser stripe is projected onto a surface and the reflected beam is detected by CCD cameras. Through image processing and triangulation method, three-dimensional coordinates are acquired. The laser probe is mounted on a three-axis transport mechanism and moves along the scan path that consists of a series of predetermined line segments. It also rotates in two directions.

When the laser scanner captures an image, the system automatically finds an optical focus and keeps the standoff distance. The length of laser stripe and the stand-off distance cannot be changed by an operator. Since a laser scanner consists of optical sensors and mechanical moving parts, various constraints must be satisfied when measuring a certain point on a part (Fig. 5). The goal of this section is to generate an optimal scan plan that satisfies the following major constraints (Zussman et al., 1994):

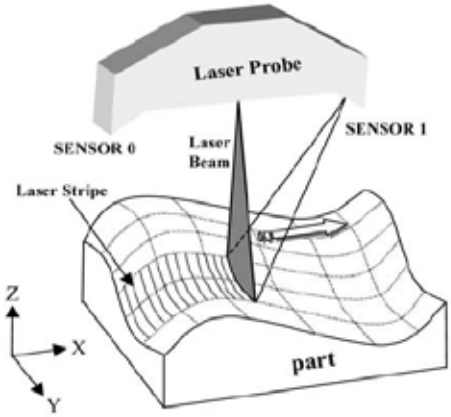

Fig. 4. Laser scanning mechanism

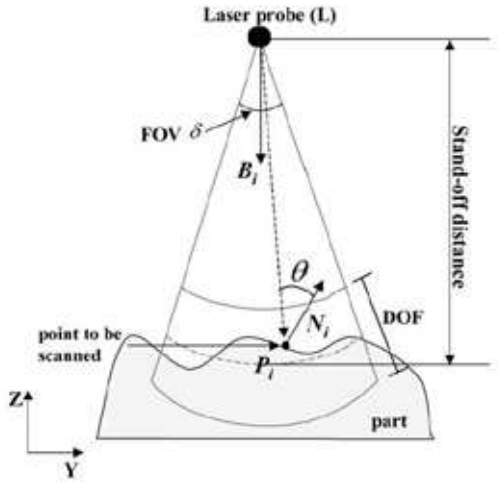

Fig. 5. Constraints for laser scanning

1. View angle: the angle between the incident laser beam and the surface normal of a point being measured should be less than the maximum view angle γ

$$d_i \bullet N_i \geq \cos(\gamma), \tag{1}$$

where

$$d_i = \frac{L - P_i}{|L - P_i|}. \tag{2}$$

2. FOV: the measured point should be located within the length of a laser stripe

$$\left(-d_i\right) \bullet B_i \geq \cos\left(\frac{\delta}{2}\right), \tag{3}$$

where δ is the FOV angle

3. DOF: the measured point should be within a specified range of distance from the laser source

$$l_{STAND} - \frac{l_{DOF}}{2} \leq \left|L - P_i\right| \leq l_{STAND} + \frac{l_{DOF}}{2}, \tag{4}$$

where l_{STAND} and l_{DOF} denotes stand-off distance and DOF length.

4. Occlusion: the incident beam as well as the reflected beam must not interfere with the part itself.
5. The laser probe should travel along a path that is collision-free.
6. If the part is shiny or transparent, preprocessing is required such as spraying.

2.2 Range error analysis of an integrated time-of-flight, triangulation and photogrammetric 3D laser scanning system

Laser scanner model (Blais et al., 2000). Models must be able to relate design parameters, laboratory measurable, and operational performance. Figure 6 illustrates the major subsystems of an active electro-optical system: projector sources and collimating optics, deflection mechanism, collecting optics, detector, signal conditioning and processing, and final output. The collecting optics images the radiation onto the detector. In the example of Figure 7, the scanner optically moves the detector's instantaneous field-of-view (IFOV) across the total field-of-view (FOV) to produce an output voltage (signal) proportional to the local scene intensity (produced by ambient light conditions) and the laser light reflected back from a reflective surface.

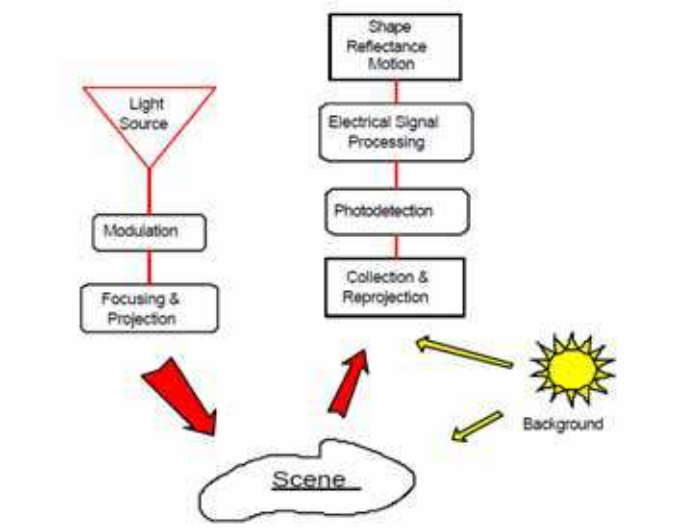

Fig. 6. Generic sensor operation applied to active electro-optical systems

The detector is at the heart of the electro-optical system because it converts the scene radiation (reflected flux) into a measurable electrical signal. Amplification and signal processing creates a signal in which voltage differences represent scene intensity differences due to various objects in the field-of-view.
The majority of electro-optical quality discussions are centered on resolution and sensitivity evaluation. System sensitivity deals with the smallest signal that can be detected. It is usually taken as the signal that produces a signal-to-noise ratio of unity at the system output. Sensitivity is dependent upon the light-gathering properties of the optical system, the responsivity of the detector, the noise of the system and, for this application, the background flux. It is independent of resolution.
In the case of metrology, resolution is not sufficient and stability and accuracy must also be considered. Resolution has been in use so long that it is thought to be something fundamental, which uniquely determines system performances and is often confused with accuracy. It is often specified by a variety of sometimes-unrelated metrics such as the Airy disk angular size, the detector subtense, or the sampling frequency. Resolution does not usually include the effect of system noise.

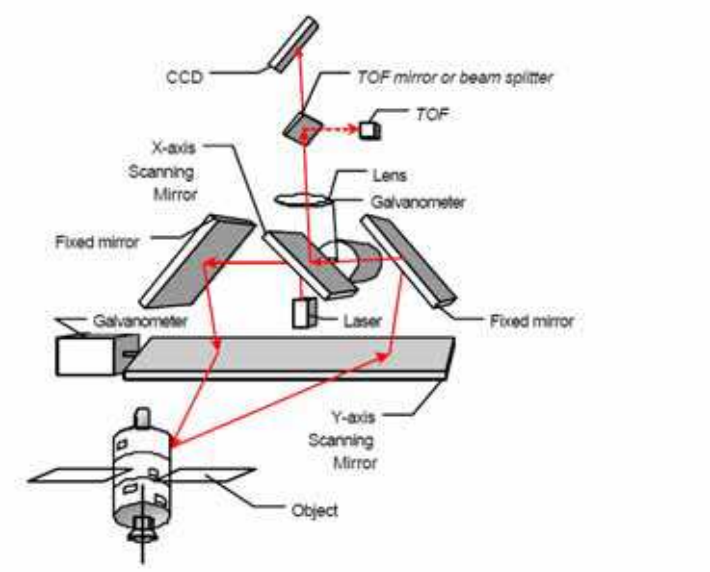

Fig. 7. Schematic representation of the auto-synchronized geometry

2.3 The auto-synchronized laser scanner

Figure 7 shows a photograph of the prototype of the auto-synchronized laser scanner developed for this demonstration. The scanner uses a variation of the auto-synchronized triangulation range sensor based on one galvanometer (Blais et al., 1988). The system comprises two orthogonally mounted scanning mirrors and a linear discrete-response photosensitive position device (e.g. linear CCD) used for short to medium range measurement as triangulation (Beraldin et al., 2000). An optional avalanche photo-diode-based Time-of-Flight (LIDAR) ranging module is used for longer-range measurement

(Laurin et al., 1996). Only resolved targets using TOF are considered for this application. Laser illumination is provided using a laser source coupled to a single-mode fiber, either pulsed (TOF mode) or CW (triangulation mode). The laser scanner operates at a relatively eye safe wavelength of 1.5 mm (compared to visible laser wavelengths).
The basic concept of auto-synchronization is that the projection of the light spot is synchronized with its detection as illustrated in Figure 7. The instantaneous field of view (IFOV) of the position sensor follows the spot as it scans the scene. Therefore, an external optical perturbation can potentially interfere with the detection only when it intersects the instantaneous field of view (IFOV) of the scanner. At this level, electronic signal processing is used to filter these false readings to obtain correct 3-D measurement (Blais et al., 1991). With synchronization, the total field of view (FOV) of the scanner is related to the scanning angles of the galvanometers and mirrors as opposed to a conventional camera-based triangulation. Here the field of view and image resolution are intimately linked (Blais et al., 1988); a large field of view produces a lower pixel resolution. In summary, the instantaneous field-of-view of the scanner plays a major role in the system sensitivity analysis.

2.4 Range measurement

Figure 7 shows the optical geometry of the auto-synchronized laser scanner. The laser scanner system can measure range information for each voxel (3-D pixel) in the scene using two modes of operation: (1) triangulation as illustrated in Figure 8, and (2) time-of-flight shown in Figure 9. It is beyond the scope of this paper to discuss the details of operation of the scanner and the exact mathematical model. This information is available from previous publications where the scanner is operated in imaging mode (Blais et al., 1988; Beraldin et al., 1993; Beraldin et al., 2000). Here, we will use the simplified models illustrated in Figure 10 to model range measurement and to associate object pose estimation obtained using video camera models shown in Figures 10 and 11 and techniques discussed in section 4.

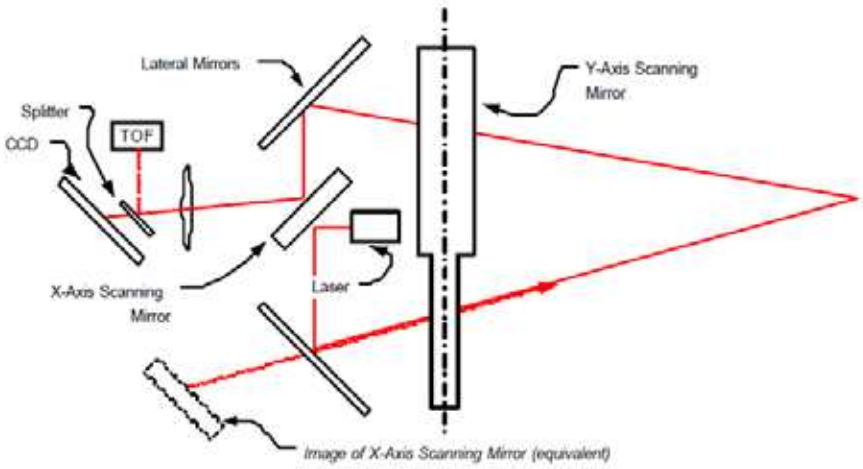

Fig. 8. Simplified geometry of the laser scanner for the triangulation mode

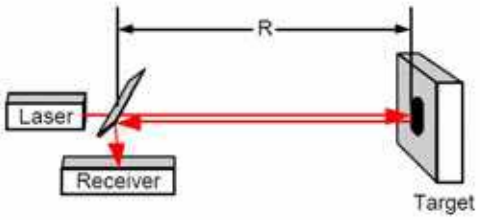

Fig. 9. Schematic of the time-of-flight principle

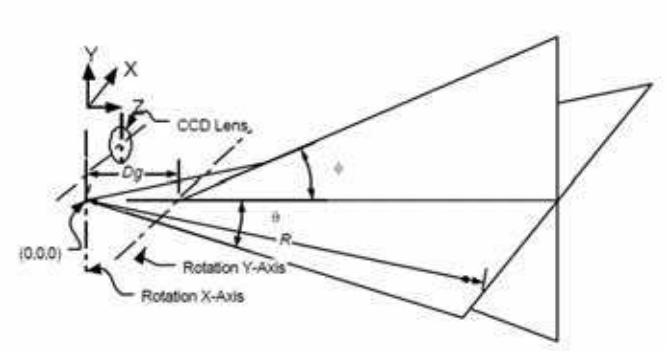

Fig. 10. Simplified geometrical model of the laser scanner showing the effect of astigmatism between the X and Y scanning axis

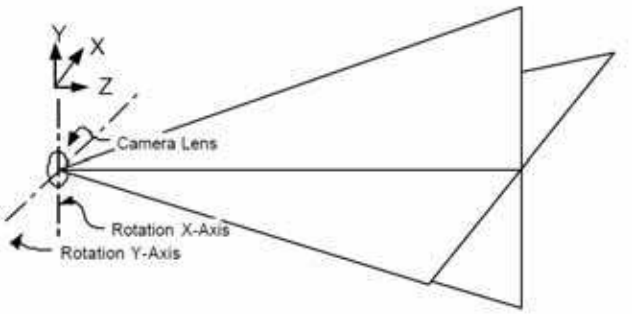

Fig. 11. Simplified geometrical model of a simple camera lens system used by conventional camera and photogrammetric methods

From (Blais et al., 1988), knowing that $R=z/\cos(\theta)$, and from Figure 10, range R can be calculated either using triangulation methods or TOF. The simplified aberrations free model is presented here. For triangulation, range is given by

$$R_{Trian} = \frac{f \cdot d}{p}\cos(\theta) + d\sin(\theta) \tag{5}$$

where f is the focal length of the lens, d is the triangulation base, θ is the deflection angle following the x-axis, and p is the position of the imaged laser spot of the position sensor (see (Blais et al., 1988) for details). For the TOF method of Figure 9, range is simply obtained based on the speed of light c and the propagation delay $\boldsymbol{\tau}$ of a laser pulse:

$$R_{TOF} = c\frac{\tau}{2} \tag{6}$$

From Figure 10, the x-y-z coordinates of a point are

$$\begin{bmatrix} x \\ y \\ z \end{bmatrix} = R \cdot \begin{bmatrix} \sin(\theta) \\ (\cos(\theta) - \psi)\sin(\theta) \\ (1 - \cos(\theta))\psi + \cos(\theta)\cos(\theta) \end{bmatrix} \tag{7}$$

where θ and φ are the deflection angles, and $\psi = Dg/R$ where Dg is the separation between the two scanning axis shown in Figure 10. Range R is obtained using either R_{Trian} or R_{TOF} depending on the operating mode of the scanner. Because Dg<<R, error propagation calculations (in triangulation mode) can be approximated by

$$\Delta R_{Trian} \approx \frac{R^2}{f \cdot d}\Delta p \tag{8}$$

$$\begin{aligned} \begin{bmatrix} \Delta x \\ \Delta y \\ \Delta z \end{bmatrix}^2 = & \begin{bmatrix} \sin(\theta) \\ \cos(\theta)\cdot\sin(\varphi) \\ \cos(\theta)\cos(\varphi) \end{bmatrix}^2 \left(\frac{R^2}{f \cdot d}\Delta p\right)^2 + \\ & + \begin{bmatrix} \cos(\theta) \\ -\sin(\theta)\cdot\sin(\varphi) \\ -\sin(\theta)\cos(\varphi) \end{bmatrix}^2 R^2 \cdot \Delta\theta^2 + \begin{bmatrix} 0 \\ \cos(\varphi) \\ -\sin(\varphi) \end{bmatrix}^2 R^2 \cos^2(\theta) \cdot \Delta\varphi^2 \end{aligned} \tag{9}$$

where Δp is the uncertainty associated with the laser spot measurement.

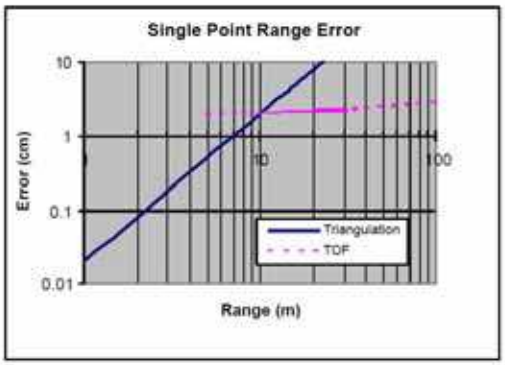

Fig. 12. Range error accuracy of the Laser Scanner System

Figure 12 shows range error measured with the scanner in triangulation (notice the R^2 dependence of the error), and from the manufacturer specifications for the TOF mode of operation (notice the almost flat error over range). Other typical system parameters for the prototype used in Figure 7 are maximum deflection angles of 0.5 rad (30 deg) and angular errors of 50-100 μrad, depending on the target array. From equation 9 and Figure 12, the total system error, for medium to long range, is mostly contributed by range error measurement ΔR, i.e., Δp the uncertainty associated with the laser spot measurement.

2.5 Traversable terrain classification for outdoor autonomous robots using single 2D laser scans

Autonomous navigation by mobile robots in unstructured or semi-structured outdoor environments presents a considerable challenge (Andersen et al., 2006). Adequately solving this challenge would allow robotic applications within industries such as agriculture, mining and logging. To achieve the level of autonomy required for such operation, a robot must be able to perceive and interpret the environment in a meaningful way. Limitations in current sensing technology coupled with a dynamically changing unknown environment, and difficulties in modeling the interaction between robot and terrain all make this task difficult.

The sensors used for this task could include vision, ultrasound, radar and laser scanner, both as combined solutions and each sensor type used individually. Multi sensor solutions would be expected to provide superior results but computational efforts and requirements of fast real-time classification make it interesting to explore what would be achievable with a single sensor.

Current work in the area tends to focus on using 3D laser scanners, vision or a combination of 3Dlaser scanners and vision. In vision solutions (Bertozzi & Broggi, 1997) argues that this problem can be divided into two sub-problems: Lane following and obstacle detection, and describes a stereo vision based solution for both. Edge detection in vision systems is one of the possibilities to identify road borders and had some success already in 1986 as described in (Wallace et al., 1986), color segmentation is used in (Fernandez & Price, 2005) for tracking of dirt roads, road types similar to the ones used in this paper. A method for road following using vision and neural network was developed by (Jochem et al., 1993). A combined stereo vision and 2D laser scanner solution for outdoor obstacle avoidance is presented in (Pagnottelli et al., 2005). Using 3D laser scanner solutions have been proposed by (Vandapel et al., 2004) by transforming point clouds into linear features, surfaces, and scatter. These were classified using a Bayesian filter based on a manually classified training set. Identification of navigable terrain using a 3D laser scanner by checking if all height measurements in the vicinity of a range reading had less than a few centimeters deviation is described in (Montemerlo & Thrun, 2004). An algorithm that distinguished compressible grass (which is traversable) from obstacles such as rocks using spatial coherence techniques with an omni-directional single line laser was developed by (Macedo et al., 2000). A method of traversing a rock field based on three metrics extracted from stereovision was likewise developed by (Wettergreen et al., 2005). A tactile and vibration-based approach to terrain classification was proposed by (Legnemma et al., 2004). A method for detection and tracking the vertical edges of the curbstones bordering the road, using a 2D laser scanner, was developed by (Wijesoma et al., 2004). Detection of borders or obstacles using laser scanners are often used both indoors and in populated outdoors environments, and is the favored method when the purpose includes map building, as in (Guivant et al., 2001; Klöör et al., 1993).

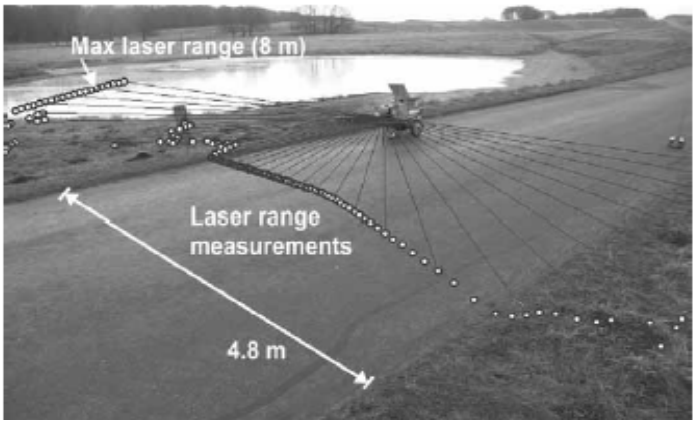

Fig. 13. The robot uses a laser scanner to detect the terrain in front of the robot

Fig. 14. The robot used in the experiments has a laser scanner at a height of 41 cm looking down in an angle of $\theta_L = 9°$. The road is therefore detected at 2.6 m. The position of the last scan (scan n − 1) is shown to illustrate the largest undetected obstacle. The unseen object is not detected in scan n − 1 and is too short to be seen by scan n

2.6 Constructing a 3D laser range finder

Now we will consider a three-dimensional laser range finder and its design.

The presented 3D laser range finder is built on the basis of a 2D range finder by extension with a mount and a servomotor. The 2D laser range finder is attached to the mount so that it can be rotated. The rotation axis is horizontal. A standard low-cost servomotor is connected on the left side (fig. 15).

It is an alternative approach if we have to rotate the range finder around the vertical axis. In (Surmann at al. 2001) it is only discussed the approach based on a horizontal rotation, but all presented algorithms can be used in the same way. The differences between both approaches are the orientation of the apex angle and the effects of dynamic objects moving through the scene, e.g. persons. Using vertical scanning, a perturbation either appears with low probability within a few scans making them useless for further data processing, or does not appear at all. The first approach on the other hand shows perturbations throughout the whole scene, but these data can still be used for robot navigation and object detection.

Fig. 15. A 3D laser range finder for autonomous mobile robots. The servo is mounted at the left side. A camera on top is used to get texture images for the realistic appearances of a 3D scene (Surmann at al. 2001)

The given setup determines an intrinsic order of the acquired data. The data coming from the 2D laser range finder is ordered anticlockwise. In addition the 2D scans (scanned planes) are ordered due to the rotation. A digital camera for texture mapping is mounted on top of the 3D laser range finder. While rotating, several photos are taken so that the texture mapping can be applied to a larger area. The 3D laser range finder uses only standard interfaces of a computer. The servomotor is directly connected to the parallel port, the 2D laser range finder to the serial port and the camera is connected to an USB port. Nowadays, every computer (esp. laptops) does have these interfaces and the built 3D laser range finder can therefore easily be used on mobile platforms. The mount and the servo are inexpensive and no special electronic devices are used, so the price of the whole system mainly depends on the used 2D laser range finder.

3. Typical constraints of laser scanners constructions

As evident from above analysis, in the different laser scanner constructions by its nature are involved the next typical constraints and limitations:

- a limited geometry of the field-of-view with non-uniformly distributed uncertainty of the sinus law application (Zussman et al., 1994), (Montemerlo & Thrun, 2004), (Sergiyenko et al. [a]; 2009), (Sergiyenko et al. [b]; 2009).
- non-uniform spatial distribution of the scanning tool – laser ray – along the variable striking distance (Guivant et al., 2001; Klöör et al., 1993) , (Surmann at al. 2001);
- not balanced torque of the rotating electromechanical system; wear process of friction surfaces and rocking of electromotor shafts (Surmann at al. 2001), (Pagnottelli et al., 2005);
- unwanted quaziperiodical noise of the complex nature in a photodetecting circuit (Básaca [a] et al., 2010);
- limited range of action due to non-lineal photodetected signal attenuation (Sergiyenko et al. a; 2009), (Sergiyenko O.Yu.; 2010).

The most prospective ways of the mentioned constraints decrease is a subject under consideration it the further sections.

4. Limitations decrease of the field-of-view geometry design

As we can observe from the several different laser scanner constructions mentioned above, they have a common point: for general compactness of device the emitter and receiver are located very closely to each other. But it is well known that for small angles a trigonometric function of sinus/tangens are approximately equal to the angle because of linearization of the trigonometric functions (truncation of their Taylor series). In our task these functions are the basic for used mathematical formalism. Hence, it causes non uniform resolution of the theoretical method inside a full field-of-view of the system. The same reason causes a problem of resolution at the angles close to 90º.
Experimental proofs of such non-uniform uncertainty distribution are shown in (Rivas Lopez et al. [a], 2008), (Rivas Lopez et al. [b], 2008), (Rivas Lopez et al. , 2010), (Sergiyenko et al. [a]; 2009). See Fig. 16.

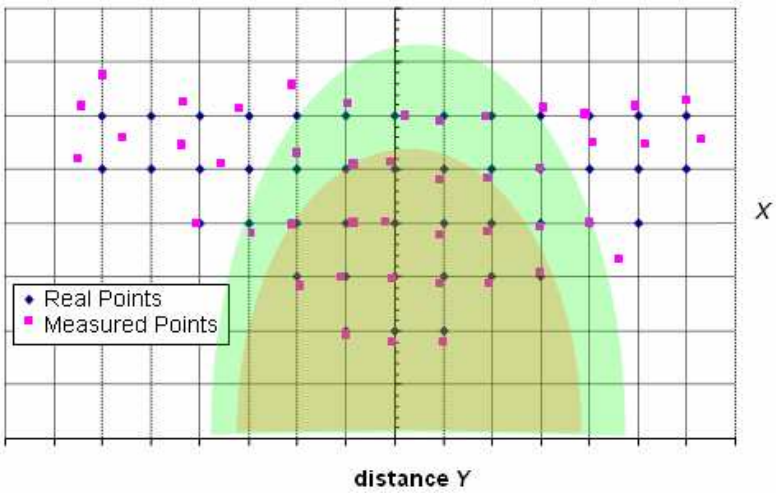

Fig. 16. Experimental graphic of point's measurement in 2D at variable obstacle positioning. TVS field-of-view and "accuracy zones", according to (Rivas Lopez et al. [a], 2008)

The accuracy of coordinates measurement is not uniform (see Fig. 16) in all TVS field-of-view, but in the olive- and green-zone correspondingly it is not more than 1% and 4% out of level of confidence (Rivas Lopez et al. [a], 2008), (Rivas Lopez et al. [b], 2008). Usually, modern regular step drives are operated with average velocity of 1 KHz. It means that we can obtain coordinates at least of 1000 points per second, each X, Y, and Z with metrological accuracy and defined uncertainties. This is a point to apply this TVS as input data sensory system.
Additionally, it is obviously that a triangulation base of 1m (used in mentioned publications) not just permits an optimal design of the optoelectronic system field-of-view, but also permits increase a computation speed for used trigonometric mathematical formalism because multiplication for 1 is an empty operation.

5. Geometrical centre search of the laser spot projection

The laser ray as the scanning tool of any laser scanner unfortunately has a non-uniform spatial distribution along the variable striking distance. This circumstance unfortunately

causes that a shape and size of the laser spot projection on the scanning surface is significantly variable. It is shown in (Sergiyenko et al. [a]; 2009), (Rivas Lopez et al., 2010), and on the Fig.17.

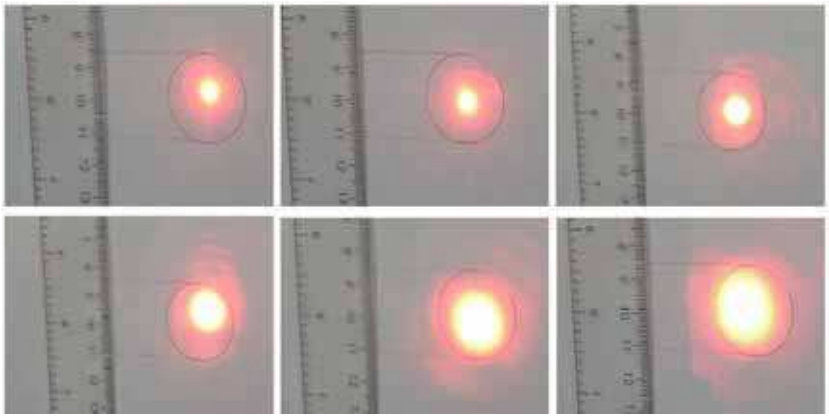

a)

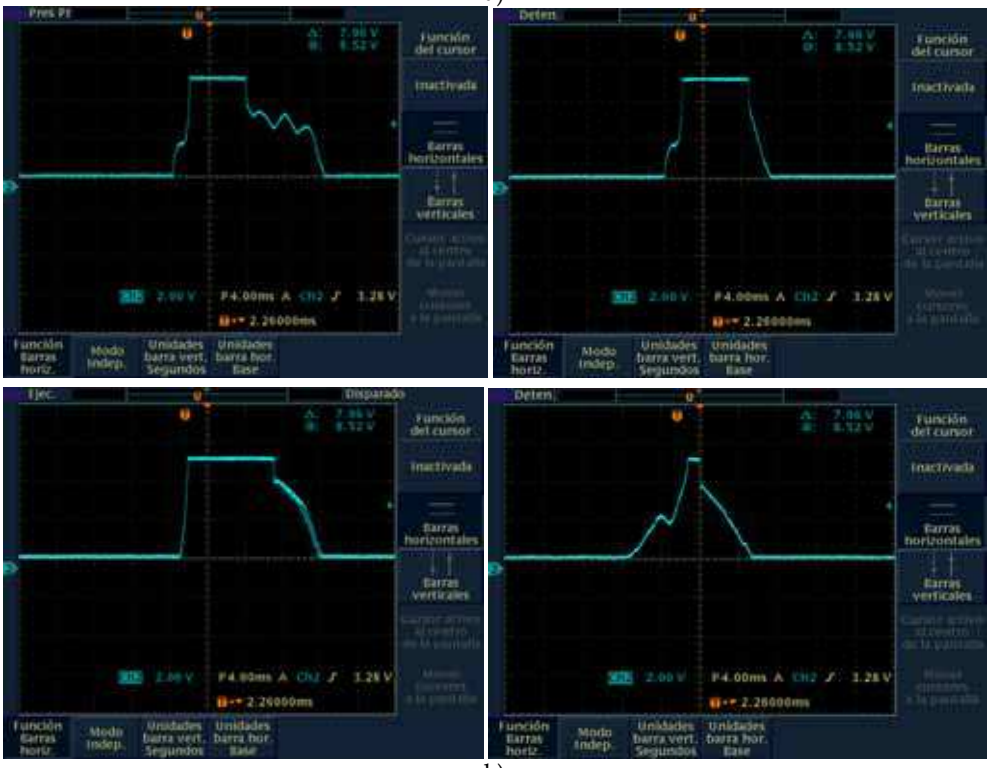

b)

Fig. 17. General view of the stop-signal at the different distances and highlighted spot sizes: a) spot sizes variation; b) stop-signal screenshot

It causes that spatial resolution of any method based on the spatial position estimation by such signals registration has a strong source of uncertainty.
The possible way for this disadvantage decrease is based on the theoretical method and special circuit of the signal energetic center search introduced in (Sergiyenko et al. [a]; 2009), (Rivas Lopez et al., 2010).

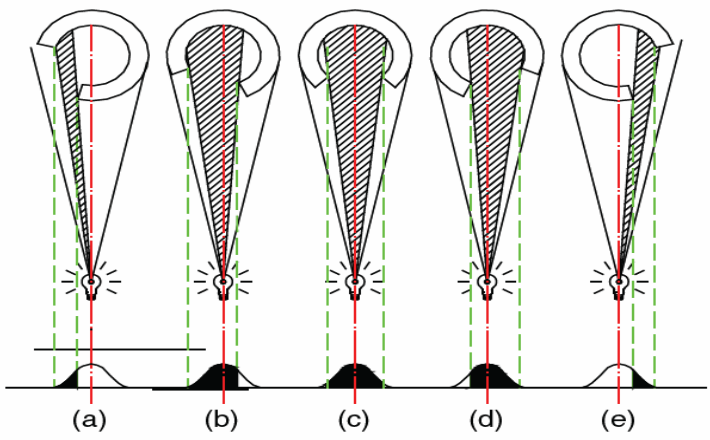

Fig. 18. The principle of noisy electrical stop-pulse formation during rotational scanning

The triangulation mathematic framework is still strongly theoretical. Because in the geometrical scheme we considering a pure geometrical objects, i.e. the straight line is precisely straight, without any curvature, have only length, all another sizes are zero; points have no any sizes and its location is characterized only by three Cartesian coordinates in the space.
Practically it is different (Rivas Lopez et al. , 2010). The optical ray it is a cone in general or even more complex shape depending on medium properties. The vertex of this cone also isn't a point, but distributed in some small spatial scope. The divergence inside this cone it is caused by many natural factors. It causes that practically the stop-pulse in photo receiver is not a short pulse of the standard form, but it is formed as shown on Fig. 18 (a-e).
It growth (Fig. 18, a) and falling down (Fig. 18, e), and fluctuating around its maximum area in figs. 18 (b-d). Taking to account the presence of some natural noise (as rule, white Gaussian noise) in this process, we can conclude that finally we need to operate the single electric signal of non-regular shape presented on Fig.19, a. Moreover, the shape and the width of this pulse are closely related to scanning velocity. But the scanning velocity in practical case is not a constant also. In this case the best problem solution is adequate signal processing. And our contribution is based on simple idea. What is it the red point on the Fig. 19, a? In the point of view of electric signals area on the graphic limited by signal curve is the energy transferred by this electric signal. So, this red point with certain small uncertainty is the signal energetic center. It is essential to note that position of the energetic center coincides for both pulses on the Fig. 19, a: ideal theoretical square pulse, and its real noisy performance. Much more essential is to note in this case, that the energetic center position uncertainty the less depends on noise, than becomes more the pulse area. In our task is the same like less scanning velocity.

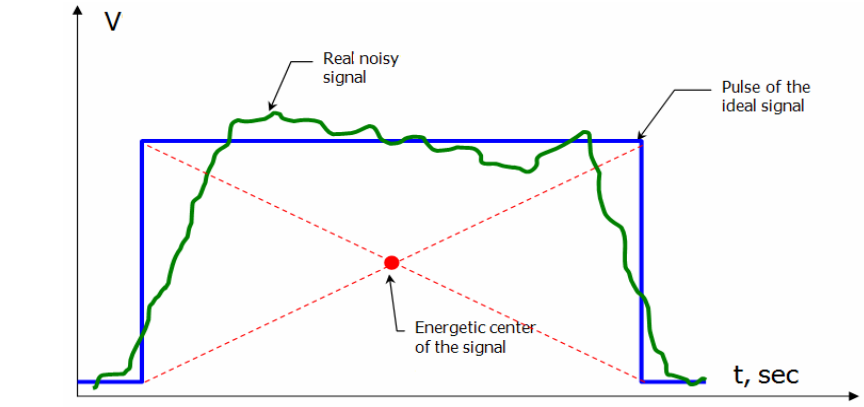

a)

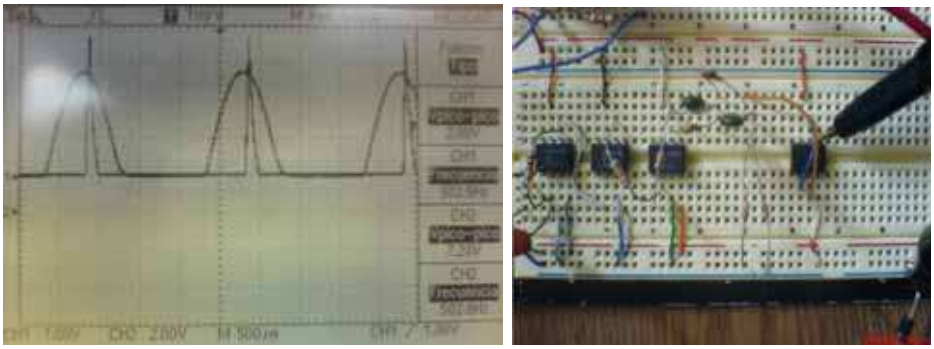

b)

Fig. 19. Method of the signal energetic center search: a) general purpose; b) differentiator circuit & functioning screenshot

From the other hand, as we consider this pulse as the optic blur equivalent registered by photosensor, it is the center of optical ray spatial cone. Such way we can detect in noisy electric signal the truth position of the unique straight line which belongs the same time the center of light source (active target) and the center of photoreceiver.

It is possible to provide practically using another strong and simple rule: the function (signal curve) maximum it is always where its derivative is zero. In another words, after finding the zero-cross position of first derivate function of the registered signal, we can find a real position of the EB in our coordinate system.

The practical realization of described operation it is possible in a several ways. However, in our primary experimentation we realize this operation using standard differentiator circuit (Fig.19, b). On the operation screenshot on Fig. 19, b it is clear evident that it is completely possible in a real time scale to obtain an electrical mark of the real light source position. Of cause it is a certain delay between real maximum position and its mark by pin-pulse (Fig. 19, b) because of differentiator circuit operating time. But it is strongly evident that it has a constant character and can be eliminated on the processing stage by simple correction factor.

6. Optimal design of laser scanner mechanical part

Serious problems of scanner normal functioning and sources of spatial resolution uncertainty are caused by not balanced torque of the rotating electromechanical system; mechanical movements delay; wear process of friction surfaces; rocking of electromotor shafts, etc.

The optimal design of the mechanical part is given in (Básaca [a,b] et al., 2010), it permits significant decrease of the most important electromechanical lacks of the previous prototype presented in (Sergiyenko et al. [a - c]; 2009), (Rivas Lopez et al. [a,b], 2008), (Rivas Lopez et al. , 2010).

(a) Prototype I system view (b) Positioning Laser (PL) (c) Scanning Aperture (SA)

Fig. 20. Prototype I

(a) Full Size Prototype II system view (b) Positioning Laser (PL) (c) Scanning Aperture (SA)

Fig. 21. Prototype II

Figure 20 shows Prototype I, this system was the first we built to demonstrate our method and although testing and experimentation were successful, we detected uncertainty points (See Fig. 17) that could be eliminated with an improved mechanical design.

Prototype II shown in Fig. 21, a, has several advantages in comparison to its predecessor; the most important is that in the new design most of the components, including the Laser are installed inside a cylindrical tube, thus placing the center of gravity in the center of the tube and providing an easier and more precise way of rotating the tube than the band used in Prototype I (see Fig. 20, a).

In other words this improvement decreases the TVS own torque which provide us with several advantages over Prototype I such as:

- The possibility of using an electric motor rated with lower torque, voltage and current per phase consumption.

- As a result, full system power consumption is reduced.
- Extended battery life which is essential for mobile applications.

Moreover, cross-comparing Fig. 20, b and Fig. 21, b and the pair Fig. 20, c - Fig. 21, c, in the constructions of PL and SA, the following improvements are presented.

The older Positioning Laser design used a fixture with a 45° mirror attached to the laser to redirect the laser beam in a 90° angle to a second 45° mirror which is attached directly to a stepper motor (Fig. 20, b). This motor is controlled to redirect the laser beam orthogonally to scan the area in front of the mobile robot.

On the other hand, the new PL design (Fig. 21, b) is based on the same general principle but has mechanical differences. E.g. the new PL has no fixture attached directly to the laser; instead of attaching the 45° mirror, part of the inside surface of the cylindrical tube is machined with mirror finish, with this, the possibility of uncertainty due to mirror displacement or improperly installed fixture is eliminated. It is the way to decrease the uncertainty deviation on Fig.17.

Another uncertainty source is that the more far away the surface marked by the laser, the greater the laser beam or spot diameter becomes. Fig 20, b shows that the laser beam travels a certain distance and is redirected by a mirror on two occasions, due to this travel, at the PL output the laser beam diameter is already greater than the originally emitted laser beam diameter.

Hence, another improvement is that the distances between the laser and the mirrors, i.e. the laser beam travel was reduced from centimeters to millimeters, by doing this the laser beam diameter in the PL output equals to the beam diameter emitted from the laser output, maintaining the lowest beam diameter possible within the TVS, therefore theoretically increasing the TVS range. Analysis of laser spot diameter variation is given in (Básaca [a,b] et al., 2010), it shows that this circumstance plays a significant role in total uncertainty distribution, and this part of general design is critical for total uncertainty decrease.

The Scanning Aperture design is maintained from Prototype I to II (Fig 20, c and Fig 21, c), the only difference is that the new SA is smaller in size and is installed within the cylindrical tube, however it's important to mention that the most critical point with the SA is to maintain it aligned in the same plane as PL in order to be able to create the dynamic triangle more solid or fixed in mechanical meaning, i.e. only this design guarantee that scanning ray and scanning plane are meeting exactly in the same plane triangle.

7. Noise filter for photoreceiver circuit

Experimental studies of electromechanical laser scanner prototype as the rule shows the presence of noise of the complex nature in a photodetecting circuit. It is caused by cross-action of two main components: mechanical vibration and, properly, optical noise.

The typical procedure of the filter design for such kind of noise, for different scanning velocities, will be introduced in full text of this paper basing on the material of publication in (Básaca [a] et al., 2010).

One of the most challenging points of normal TVS functioning is the presence of typical input noise mixed with the "stop-signal" train in the form of the screenshot on Fig. 22. This noise can be filtered by specially designed circuit (Fig. 23) with the aim of guaranteed detection of true position of the scanning ray reflected points, in other words the guaranteed localization of the real "stop-pulses".

As in every system, noise is present here too in the signal acquired from the photo receiver, after studying the signal we observed that the noise reaches maximum amplitude of 120 mV (see Fig. 22) with frequencies that vary between 400 Hz and 20 KHz. To eliminate this noise a Butterworth third order low pass filter (-60 dB per decade) was designed and implemented, see Fig. 23. The filter's output connects to a voltage level detector with a reference voltage of 120mV to reject the noise amplitude, whenever an obstacle is detected by the photo receiver a spike in the signal is detected, the voltage of this spike varies depending on the distance of the detected obstacle but is always greater than 120mV from the noise amplitude. The output of the voltage level detector is a signal of 5Vdc when an obstacle is detected and remains at 0Vdc when there is no obstacle, in other words providing us with a 0-5Vdc square signal which indicate us whether an object is present or not.

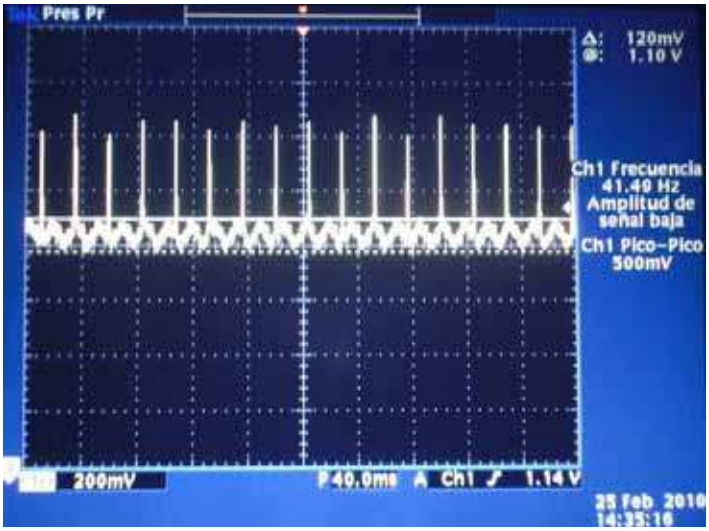

Fig. 22. Typical experimental noise voltage and frequency

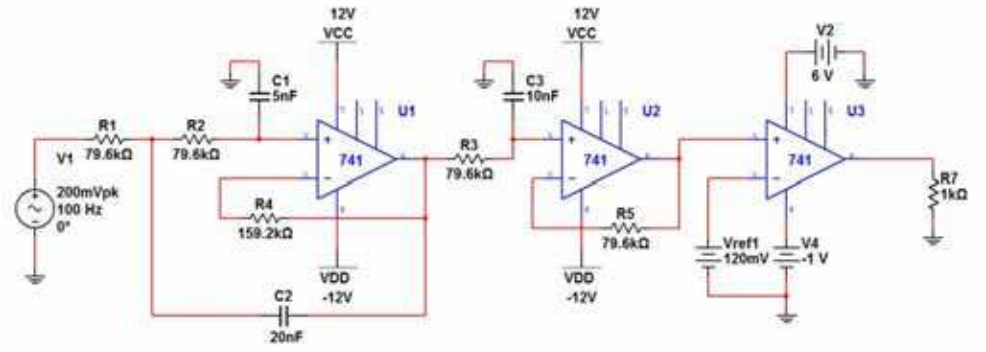

Fig. 23. Butterworth third order low pass filter (-60 dB/decade) and voltage level detector

The Butterworth type filter was chosen over other types such as Chebyshev filters due to Butterworth's more linear phase response and flat frequency response in our passband according to (Coughlin & Driscoll, 1999). Our filter was designed as follows:

$$\omega_c = 200;\ C_3 = 10nF \tag{10}$$

where ω_c is the cutoff frequency, the value assigned is 200 Hz in order to let pass the frequency band between 0 and 200 Hz, letting pass the signal of a detected obstacle and attenuating all the frequencies higher than 200 Hz.

$$C_1 = \frac{1}{2}C_3 = 5nF \tag{11}$$

$$C_2 = 2C_3 = 20nF \tag{12}$$

$$R = \frac{1}{\omega_c C_3} = \frac{1}{(6.25)(200)\left(5x10^{-9}\right)} = 79.617k \tag{13}$$

$$R_1 = R_2 = R_3 = R = 79.617k\Omega \tag{14}$$

$$R_{f1} = 2R = 159.235k\Omega \tag{15}$$

$$R_{f2} = R = 79.617k\Omega \tag{16}$$

The filter with -60 dB/decade attenuation is achieved by cascading a -40 dB/decade filter and a -20 dB/decade filter. The total closed loop gain is the multiplication of each filter's gain. See Fig. 23 for the frequency response of the circuit shown on Fig. 23, (Coughlin & Driscoll, 1999).

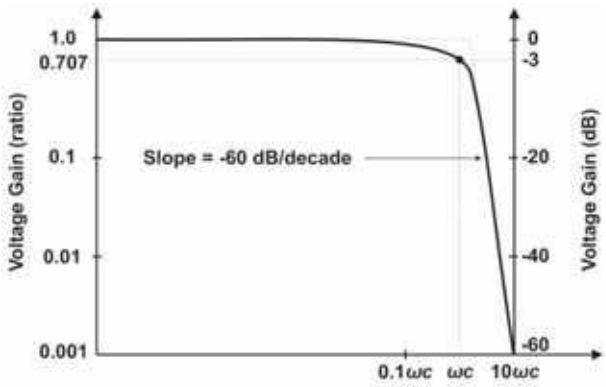

Fig. 24. Frequency response for Butterworth third order low pass filter (-60 dB/decade)

7.1 Simulation

The circuit presented on Fig. 23 was simulated with software from National Instruments, NI Multisim 10. Fig. 25, a shows a caption of a Simulated Tektronix Oscilloscope with three

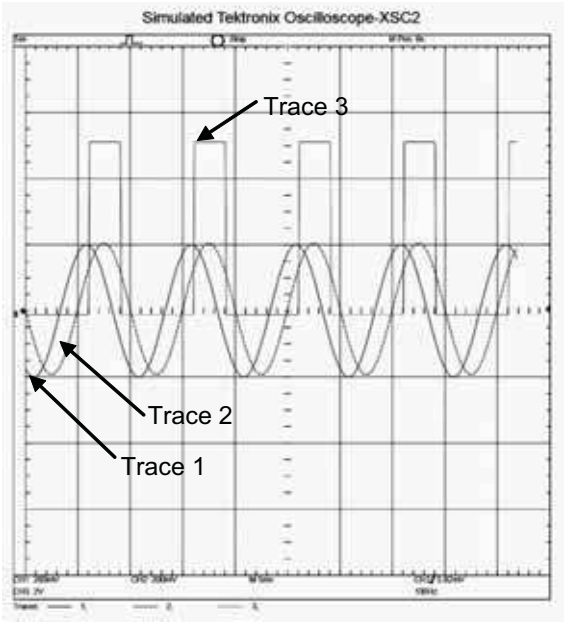

(a) Input signal is 200mV at 100 Hz; output is a 0-5Vdc square signal

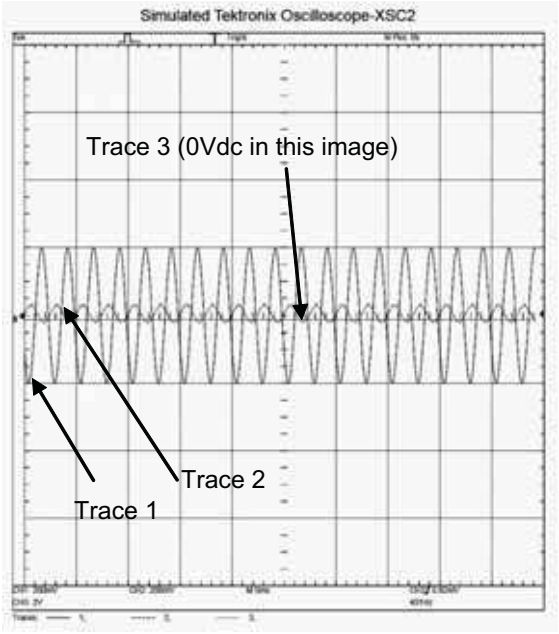

(b) Input is 200mV at 400 Hz; output is attenuated due to input frequency being higher than cutoff frequency (200 Hz), regardless of the input voltage.

Fig. 25. Low pass filter and voltage level detector output (circuit on Fig. 23)

signals, trace 1 is the circuit input signal that simulates the photo receiver output, this is the signal that is filtered and amplified, for this simulation the input signal is 200mV at 100 Hz. Trace 2 is the filter output, as shown below, the signal has the same amplitude as the original as long as its frequency is in the passband region (below 200 Hz), therefore it's not attenuated, it also has a delay of 8ms which is acceptable. And the last, trace 3, is the voltage level detector output, this signal will be 5Vdc if the signal voltage coming from the filter is greater than Vref (120mVdc), meaning an obstacle has been detected, and it remains 0Vdc if there is no obstacle in sight.
Fig. 25, b shows the case when the input signal is 200mV at 400 Hz, this frequency is in the stopband region (higher than 200 Hz), for this reason the trace 2 signal which is the filter output is attenuated to 35mV that for this purpose equals 0V. Therefore trace 3 remains at 0Vdc.
Thus, our simulation demonstrates that the designed filter can attenuate the experimentally detected undesired noise in TVS prototype above 400Hz.

7.2 Slower scanners for application in medical surgery

At the more slow scanning, which permits increase the resolution in spite of operating time, it was experimentally obtained the noise of same character, but with another typical values. Such scanning velocity decrease it is expedient, for example, for medical scanners application (Rodriguez et al., 2009).
The dead zone circuit DZC Fig. 28 cut any signal that is greater than 200mV; this eliminates any noise left over after applying the filter of -40db. The detected signal corresponding to the laser is greater than 400mV which allows the cut rise. In experimentation is carried out that useful signal is berried in noise, wish have in our case a typical form presented on Fig. 25. With the aim to delete this noise in this paper design DZC under consideration. After DZC we make a saturation of the signal and amplify to 5 Volts, thereby obtain a processable signal to detect the moment of triangulation. It should be mentioned that the period of existence of the triangle can be measured in the order of a millisecond, but this time is sufficient to calculate the necessary angles.

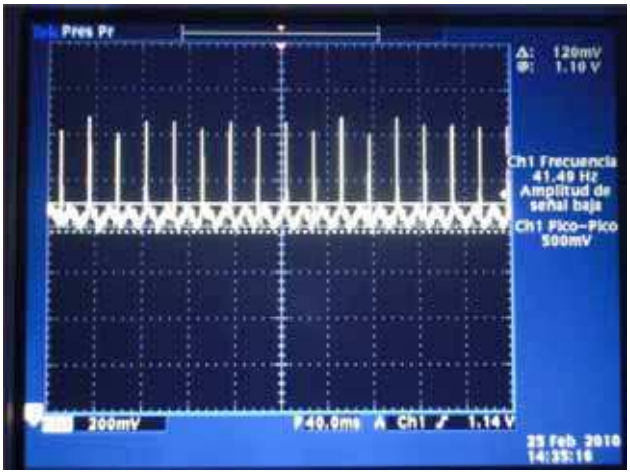

Fig. 26. 200 mv Noise, the peaks are the useful signal

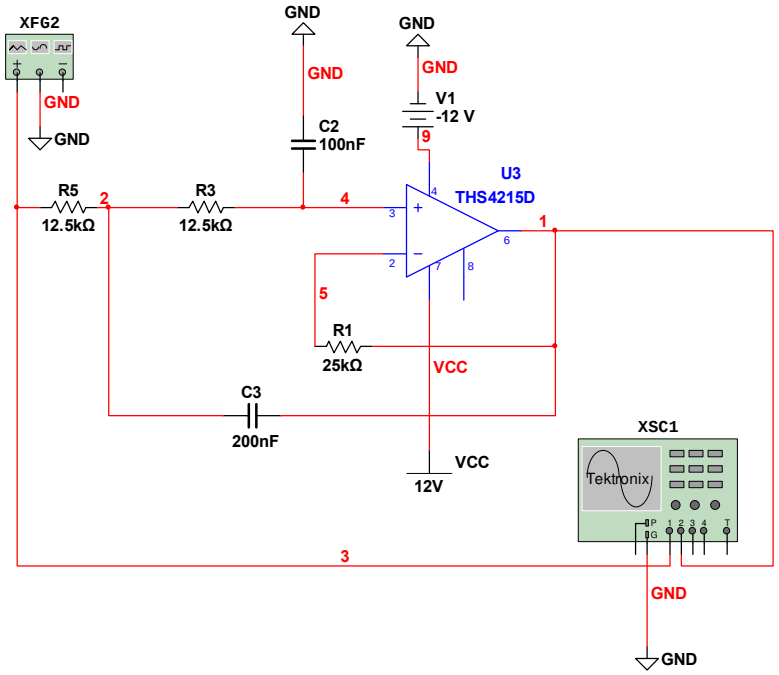

Fig. 27. Low pass Filter with -40db and fast attenuation response at 10ωc

The filter produces an attenuation of -40db/decade, after the cut-off the input magnitude decreases 40db when ω increases to a value of 10ωc Equation 18. The operational amplifier is connected so as to obtain unitary dc gain. It includes resistance R1 to the dc deviation. Since the operational amplifier circuit is a unitary gain amplifier, the voltage on C1 equals the output voltage (Coughlin & Driscoll, 1999, pp 294 – 297). The design procedure is simplified too if R3 and R5 are equal. Then follow the following equations:
Initial data

$$f_c = 90Hz \quad C_2 = 100nf \quad R_3 = R_5 = R \tag{17}$$

Cut frequency expressed in Radians/ Second

$$\omega_c = (2\pi)(f_c) \tag{18}$$

Capacitor 3 Value

$$C_3 = (2)(C_2) \tag{19}$$

Voltage Gain of the close loop

$$A_{CL} = \frac{1}{1 + j\omega RC} \quad A_{CL} = \frac{1}{1 + j1} = \frac{1}{\sqrt{2}\angle 45^{o}} \quad |A_{CL}| = \frac{1}{\sqrt{2}} = .707 \tag{20}$$

R Value using -40db as parameter

$$R = \frac{|A_{CL}|}{(\omega_c)(C_1)} \tag{21}$$

R1 Value:

$$R_1 = 2R \tag{22}$$

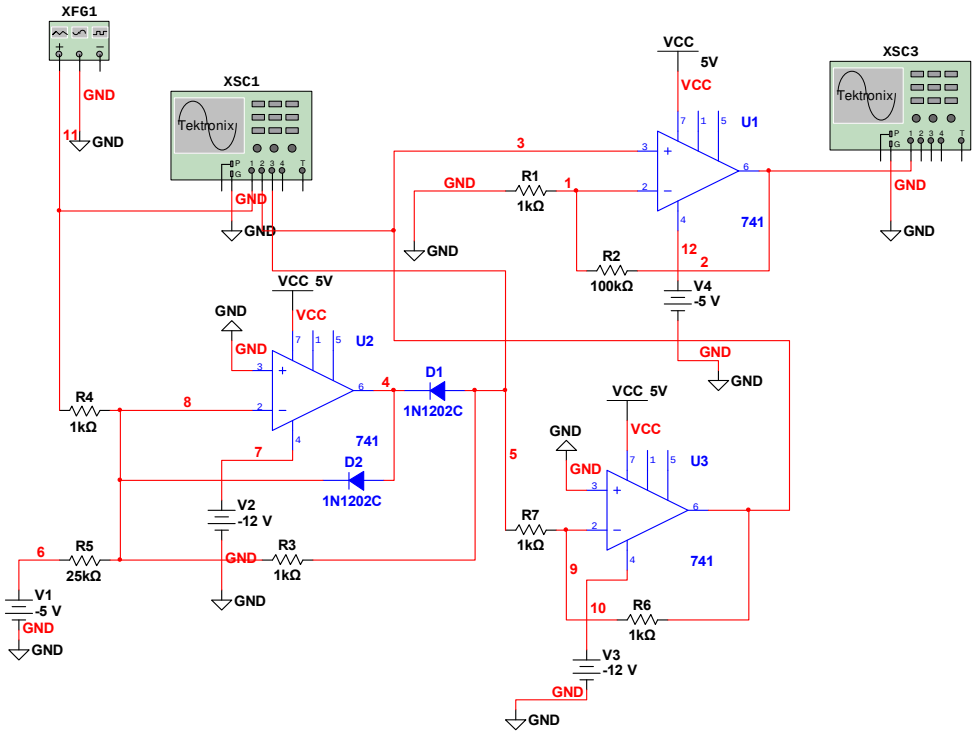

Fig. 28. Dead Zone to complement application filter circuit with saturation amplifier

Through a regulated supply voltage V1 and a resistance mR (R5) sets the reference voltage Vref. This is calculated from Equation 24. As will be shown the negative value of Vref is what defines the dead zone. The diode D2 always leads XFG1 values and set the "node 5 =- XFG1 – Vref". Whenever XFG1 exceeds the value of -Vref = 200mV, the output node 3 lets you know the amount XFG1 exceeds the value-Vref. There is a dead zone when there are values XFG1 below -Vref. (Coughlin & Driscoll, 1999, pp 200 – 204).
Initial data

$$R = R1 = R3 = R4 = R6 = R7 = 1k \tag{23}$$

Reference Voltage in the dead zone

$$V_{ref} = \frac{V_1}{m} \quad \text{(Node 6)} \tag{24}$$

Gain to be amplified and detect the signal as 0 volts or 5 volts (0 or 1 logic)

$$Gain = \frac{R2}{R1} \tag{25}$$

R5 Value

$$R5 = (m)(R) \tag{26}$$

In Fig. 30 are presented the results of simulation of the designed filter functioning. As shown Fig. 30 without a DZC the signal is not detectable (As in Fig. 26) and after DZC implementation it is eliminated undesired noise and the useful signal is clear end detectable.

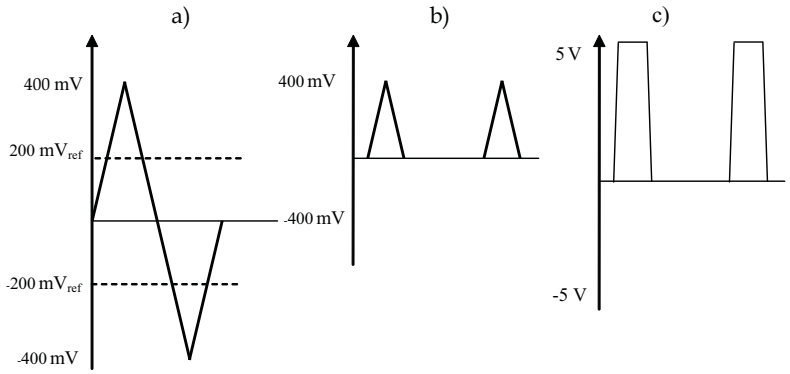

Fig. 29. a) dead zone circuit, b) Inverse Follow Circuit, c) Saturation amplifier

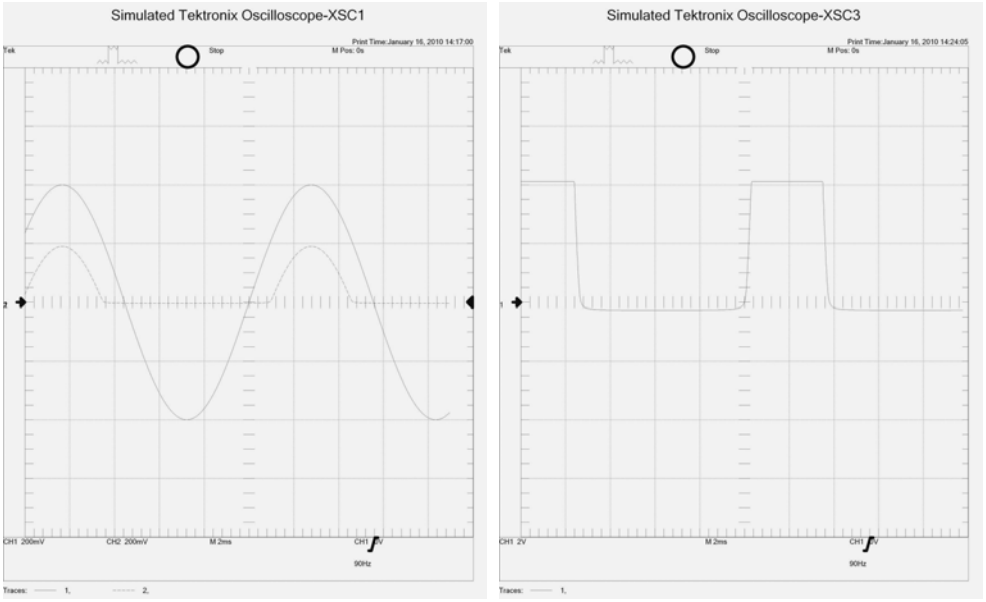

Fig. 30. Filter Output in 90 Hz Signal a) Signal as Fig. 25 without DZC b) Output Signal after DZC

8. Robust detection of the weak reflected signals

In (Sergiyenko et al. [a]; 2009), (Sergiyenko et al. [b]; 2009), (Sergiyenko et al. [c]; 2009), (Sergiyenko et al.; 2008), (Rivas Lopez et al. [a], 2008), (Rivas Lopez et al. [b], 2008), (Rivas Lopez et al. , 2010) it is shown various times that practically the most strong constraint of electromechanical laser scanner use is the signal attenuation (voltage decrease) in a photodetecting circuit. It is shown on Fig. 31:

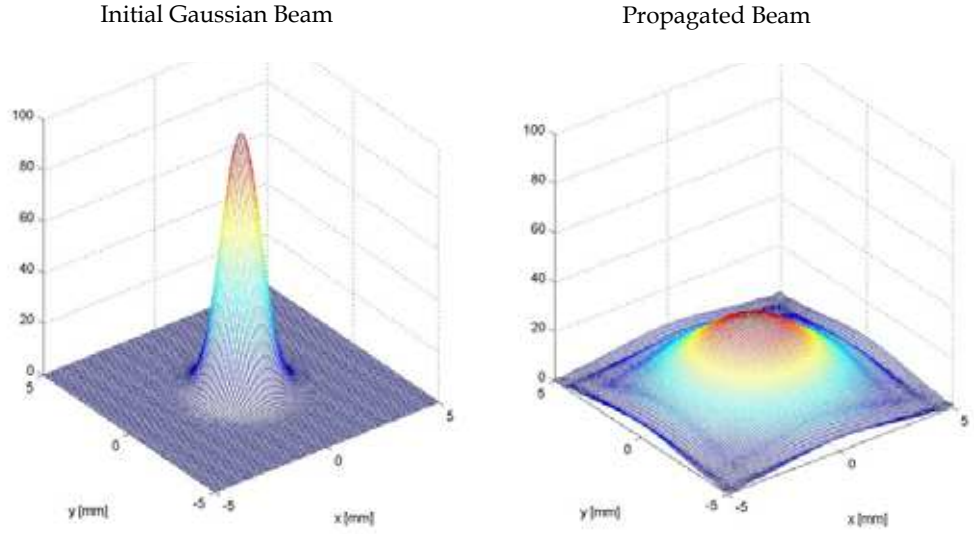

a) b)

Fig. 31. a) Power distribution pattern for 0 meter from laser source. b) Power distribution pattern for 15 meters from laser source

The possible way for this disadvantage decrease is based on the theoretical method of robust photometer circuit introduced in (Hernandez, 2007), (Hernandez [a], 2008), (Sergiyenko et al. [a]; 2009), (Hernandez [b], 2008).

In the scientific literature (Hernandez [a], 2008) on photometer circuits operational amplifiers are frequently used for photodiode monitoring. Nevertheless, most of the operational amplifier connections used in this kind of application are based on basic current-to-voltage converter circuits.

Figure 32 shows the basic circuit, in which D represents the photodiode and R_f is the negative feedback resistor used to convert the photocurrent into an output voltage linearly related to the light energy.

One of the clear advantages of the circuit shown in Fig. 32 is that it is of easy implementation. Nevertheless, on the other hand, as the diode is not forming part of the feedback loop, there is no way to compensate for disturbances, variations in temperature, structure and unstructured uncertainties in the photodiode, noise, and so on.

Therefore, it is important to place the sensor in a feedback loop able to deal with the above-mentioned problems. Figure 33 shows an example of a photometer circuit with the diode placed in the feedback loop (Hernandez, 2007), (Hernandez [a], 2008), (Hernandez [b], 2008):

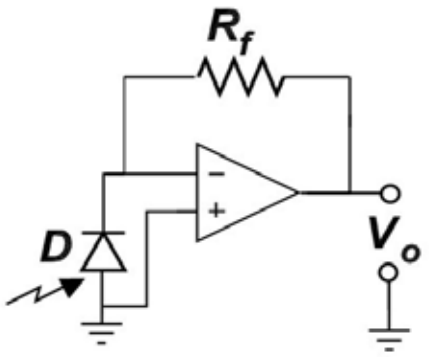

Fig. 32. Current-to-voltage converter circuit

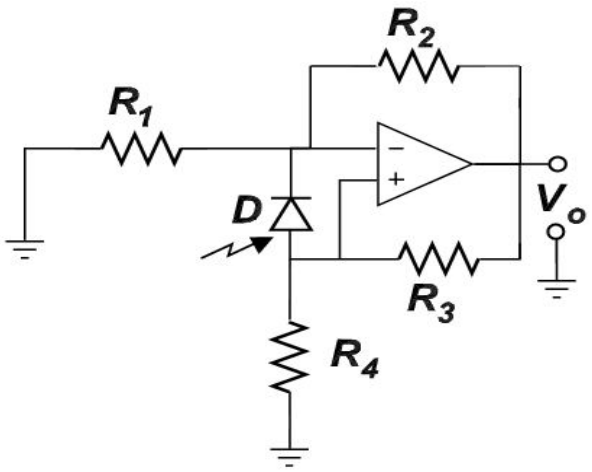

Fig. 33. Feedback photometer circuit

However, it is important to point out that in spite of the fact that the circuit shown in Fig. 33 is also of easy implementation, due to the fact that it works with positive feedback compensation it can become unstable if the values of the resistors are not chosen properly.
In (Hernandez [b], 2008), an in-depth analysis of such a circuit is carried out taking into consideration operational amplifier parameters such as the input resistance, input capacitance, open-loop gain and gain bandwidth product. Furthermore, the input-output transfer function analysis of the circuit shown in Fig.33 is carried out from the linear system theory point of view, considering that the operational amplifier is ideal.
Finally, considering the photodiode model shown in Fig. 34 (in which C_J is the junction capacitance, I_P is the light generated photocurrent, R_{SH} is the shunt resistance, R_S is the series resistance, R_L is the external load resistance and V_O is the output voltage), in (Hernandez, 2007), (Hernandez [a], 2008), (Hernandez [b], 2008) a procedure for the measurement uncertainty estimation of the circuit shown in Fig. 35 is presented.

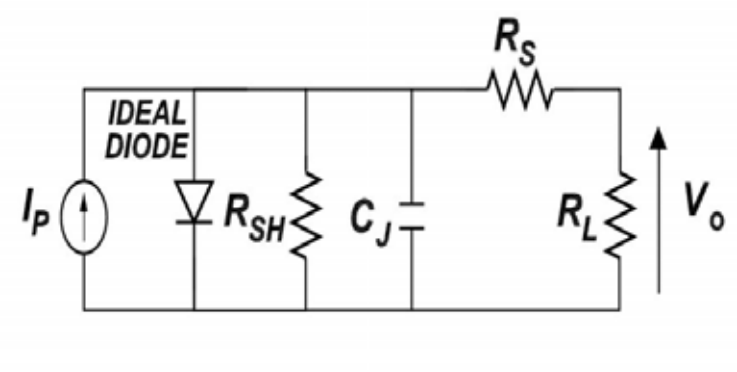

Fig. 34. Simplified version of the equivalent circuit for a photodiode

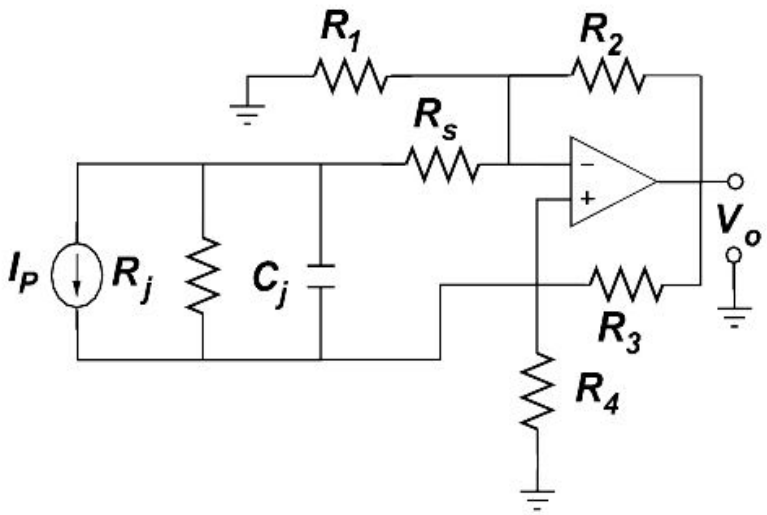

Fig. 35. Feedback photometer circuit with equivalent photodiode circuit

9. Conclusions

Finally, we can get the conclusion that possible grade of 3D scanners resolution improvements by combined application of all the mentioned actions will be efficient.

- Laser scanning systems always give a more resolution, accuracy and the better data processing time over other known Machine Vision systems. This is a reason for future research of the 3D electromechanical laser scanners for practical application matched for it in the best way. For best resolution in spatial domain it is expedient as shown above to use some additional technologies.
- Laser scanning systems always give a worse solution than other known Machine Vision systems in a part of energy consuming, medium optical conditions dependence and

range of action. So, Laser scanning systems designers always must to take in mind this fact, and to provide additional corrective measures for better system application.

- Due to non-uniform uncertainty distribution in instantaneous field-of-view (IFOV), as well in full field-of-view, it desirable the optimal geometrical design of the optoelectronic system field-of-view strictly linked to the certain practical application (i.e. static monitoring of large civil engineering structures; fast dynamic monitoring of the certain sector in indoor or outdoor autonomous robot navigation; medical scanning of the biological object with reduced movement activity; visual control of surfaces in automated assembly; etc.). In other words, the spatial sector under inspection must to be located in a smallest error sector of total TVS field-of-view. This requirement in general coincides with the basic theoretical concepts of the electro-optical system design (Fig. 5.1 on p.63 in (Wyatt, C.L., 1991)). It is expedient to note, that optimal geometrical design also permits sometimes increase a computation speed for used trigonometric mathematical formalism (for example, because multiplication or division for 1 is an empty operation).
- The use of the theoretical method and special circuit of the signal energetic center search permits us eliminate totally one of the most complex sources of uncertainty. It is uncertainty caused by irregular form and variable size of the projected light spot. It is especially important note that the variable size of the projected light spot has the non-linear relation to the distance between scanner and object surface. The uses of our theoretical method permits completely exclude this complex dependence and to establish the uncertainty rate only as a rigorous function of internal circuit parameters.
- The optimal design of the TVS mechanical part permits significant decrease of undesirable axial play, torque and wear. Mentioned above actions implementation gives a possibility to possibility of using an electric motor rated with lower torque, voltage and current per phase consumption for full system power consumption reduction and extended battery life which is essential for mobile applications.
- The typical challenging point of normal TVS functioning is the presence of input noise. As shown in the present paper, it is always necessary to realize an electronic filtration of such noise and parameters of such noise are mostly dependant on scanning velocity. Unfortunately, for this particular task only experimental test of electromechanical laser scanner prototype shows the presence of noise of the complex nature in a photodetecting circuit and its physical characteristics. It is caused by cross-action of mechanical vibration and, properly, optical noise. However, the special filter design for different scanning velocities is very similar and regular in its procedure, as it was shown in examples described in subsections 7.1 and 7.2.
- Theoretical method of robust photometer circuit introduced on photometer circuits operational amplifiers used for photodiode monitoring can permits to detect a weak signal which never been detected before in electromechanical scanners.

10. Acknowledgements

This work has been partially supported by the Autonomous University of Baja California, Mexico (projects No. 2352, in 2003-2004 and N2386, in 2005-2006) and the Ministry of Science and Innovation (MICINN) of Spain in 2009-2010 under the research project TEC2007-63121, and the Universidad Politecnica de Madrid. The authors would like to thank to various international congresses organizers, where the different aspects of the present work were

presented, for fruitful discussions and valuable remarks. The authors dedicate this work to the grateful memory of Dr. Valentin Yevstaf'yevich Tyrsa; and would like to thank to Prof. Christofer Druzgalsky and Jason McDowell (Electrical Engineering Department of California State University, Long-Beach, USA) for their invaluable assistance with English language. We appreciate also Dr. Daniel Hernandez-Balbuena's invaluable assistance in a part of discussion about uncertainty of the repetitive cyclic measurements.

11. References

Andersen, J. C.; Blas, M. R.; Ravn, O.; Andersen, N. A. & Blanke, M. (2006). Traversable terrain classification for outdoor autonomous robots using single 2D laser scans. *Integrated Computer-Aided Engineering*, Vol. 13, No. 3, 2006, 223-232, ISSN 10692509.

Básaca, L.C. a; Rodríguez, J. C.; Sergiyenko, O.; Tyrsa, V.V.; Hernández, W.; Nieto Hipólito, J. I. & Starostenko, O. (2010). 3D Laser Scanning Vision System for Autonomous Robot Navigation, *Proceedings of IEEE International Symposium on Industrial Electronics (ISIE-2010)*, Bari, Italy, July 4-7, 2010, pp.1773-1779, ISBN 978-1-4244-6390-9

Básaca, L.C. b; Rodríguez, J. C.; Sergiyenko, O.; Tyrsa, V.V.; Hernandez, W.; Nieto Hipolito, J.I. & Starostenko, O. (2010). Resolution improvement of Dynamic Triangulation method for 3D Vision System in Robot Navigation task, *Proceedings of 36th Annual Conference of the IEEE Industrial Electronics Society (IECON-2010)*, Glendale, Arizona, USA, November 7-10, 2010, pp. 2880-2885. ISBN 978-1-4244-5225-5, ISSN 1553-572X

Beraldin, J.-A.; Blais, F.; Rioux, M.; Cournoyer, L.; Laurin, D. & MacLean, S.G. (2000) Eye-safe digital 3D sensing for space applications, *Optical Engineering*, Vol. 39, No, 1, January, 2000, 196-211, ISSN 0091-3286.

Beraldin, J.-A.; El-Hakim, S.F. & Cournoyer, L. (1993). Practical Range Camera Calibration, *Videometrics II Π(Proceedings Volume)*, Sabry F. El-Hakim, pp. 21-31, Proceedings of SPIE Vol. 2067, ISBN 9780819413321.

Bertozzi, M.; Broggi, A. (1997). Vision-based vehicle guidance, *Computer*, Vol. 30, No. 7, July, 1997, 49–55, ISSN 0018-9162.

Blais, F.; Beraldin, J.-A. & El-Hakim, S.F. (2000). Range Error Analysis of an Integrated Time-of-Flight, Triangulation, and Photogrammetry 3D Laser Scanning System. *Proceedings of SPIE Vol. 4035 AeroSense 2000*, pp. 236-247, ISBN 0-8194-3661-5, Orlando, FL, USA, April, 2000, SPIE, Bellingham, Washington.

Blais, F.; Rioux, M. & Beraldin, J.-A. (1988). Practical Considerations for a Design of a High Precision 3-D Laser Scanner System, *Proc. Soc. Photo-Opt. Instrum. Eng.*, Vol. 959, 1988, 225-246, ISSN 0361-0748.

Blais, F.; Rioux, M. & MacLean, S.G. (1991). Intelligent, Variable Resolution Laser Scanner for the Space Vision System, *Acquisition, Tracking, and Pointing V (Proceedings Volume)*, Michael K. Masten & Larry A. Stockum, pp. 473-479, Proceedings of SPIE Vol. 1482, ISBN 9780819405913.

Coughlin, R. F.; Driscoll, F. F. (1999). Operational Amplifier with diodes, in *Operational Amplifier and lineal integrate circuits*, Prentice Hall, Mexico DF, ISBN 970-17-0297-0, pp 294 – 297.

Fernandez, D. & Price, A. (2005). Visual detection and tracking of poorly structured dirt roads, *Proceedings of 12th International Conference on Advanced Robotics 2005. ICAR*

'05, pp. 553–560, ISBN 0-7803-9178-0, Seattle Sheraton Hotel & Towers, July, 2005, IEEE, Seattle.

Fischer, A. (2007). Digital Processing and Fusion of 3D Data from Emerging Non-Contact 3D Measurement Technologies, In: *The future of product development*, Frank-Lothar Krause, (Ed.), pp. 387-396, Springer, ISBN: 978-3-540-69819-7, Berlin, Germany.

Guivant, J. E.; Masson, F. R. & Nebot, E. M. (2001). Optimization of the simultaneous localization and map-building algorithm for real-time implementation, *IEEE Transaction on Robotics and Automation*, Vol. 17, No. 3, June 2001, 242–257, The University of Sidney, Australia, ISSN 1042-296X.

Hähnel, D; Schulz, D. & Burgard, W. Map Building with Mobile Robots in Populated Environments. *Proceedings of IEEE/RSJ International Conference on intelligent robots and systems,* pp.496-501, ISBN 0-7803-7398-7, Lausanne , SUISSE, 30 September - 4 October 2002.

Hernandez, D.; Sergiyenko, O.; Tyrsa, V.; Burtseva, L. & Rivas López, M. (2009). Signal frequency measurement by rational approximations, *Measurement*, vol.42, issue 1, Elsevier, January 2009, p. 136-144. ISSN: 0263-2241

Hernandez, W. (2007). Robustness and noise Voltage Analysis in Two Photometer Circuits, *IEEE Sensors Journal*, vol. 7, 2007, USA, pp. 1668-1674. ISSN 1530-437X

Hernandez [a], W. (2008). Linear Robust Photometer Circuit, *Sensors and Actuators A*, vol. 141, Elsevier, 2008, p.447-453, ISSN 0924-4247

Hernandez [b], W. (2008). Performance Analysis of a Robust Photometer Circuit, *IEEE Transactions on Circuits and Systems-II,* vol. 55, No.12, December, 2008, p. 106-110, ISSN: 1549-7747

Jochem, T.; Pomereau, D. & Thorpe, C. (1993). Maniac: a next generation neurally based autonomous road follower, in F. Groen, S. Hirose and C. Thorpe, eds, *Proceedings of the International Conference Intelligent Autonomous Systems IAS-3*, pp. 592–601, ISBN 90-5199-122-3, Pittsburgh, PA, USA, February 1993, IOS Press, Pittsburgh.

Klöör, P.L.; Lundquist, P.; Ohlsson, P.; Nygrds, J. & Wernersson, A. (1993) Change detection in natural scenes using laser range measurements from a mobile robot, *Proceedings of 1st IFAC International Workshop on Intelligent Autonomous Vehicles*, pp. 71–76, ISBN 0080422233, Southampton, UK, April, 1993, Pergamon Press.

Laurin, D.; Blais, F.; Beraldin, J.-A. & Cournoyer, L. (1996). An eye-safe Imaging and Tracking laser scanner system for space Applications, *Laser Radar Technology and Applications (Proceedings Volume)*, Gary W. Kamerman (Ed.), pp. 168-177, Proceedings of SPIE Vol. 2748, ISBN 9780819421296.

Legnemma, K.; Brooks, C. & Dubowsky, S. (2004). Visual, tactile, and vibration-based terrain analysis for planetary rovers, *Proceedings of IEEE Aerospace Conference 2004*, Vol. 2, March, 2004, 841–848, ISSN 1095-323X.

Macedo, J.; Matthies, L. & Manduchi, R. (2000) Ladar-based discrimination of grass from obstacles for autonomous navigation, *Proceedings of Experimental Robotics VII ISER 2000*, pp. 111–120, ISBN 3-540-42104-1, Waikiki, Hawaii, December, 2000, Springer, Waikiki.

Montemerlo, M. & Thrun, S. (2004). A multi-resolution pyramid for outdoor robot terrain perception, *Proceedings of the Nineteenth National Conference on Artificial Intelligence AAAI-04*, pp 464–469, ISBN 978-0-262-51183-4, San Jose, California, at the San Jose Convention Center, July, 2004, AAAI Press, San Jose, California.

Nüchter, A. (2007). 6D SLAM - 3D Mapping Outdoor Environments, in: Quantitative Performance Evaluation of Robotic and Intelligent Systems, *Journal of Field Robotics*, Vol. 24, No. 8-9, November, 2008, pp. 699-722, ISSN 1556-4959

Nüchter, A. (2008). Towards semantic maps for mobile robots, *Robotics and Autonomous Systems*, *Elsevier,* Vol. 56, No. 11, November, 2008, pp. 915-926, ISSN 0921-889.

Pagnottelli, S.; Taraglio, S.; Valigi, P. & Zanela, A. (2005). Visual and laser sensory data fusion for outdoor robot localisation and navigation, *Proceedings of 12th International Conference on Advanced Robotics 2005. ICAR '05*, 171–177, ISBN 0-7803-9178-0, Seattle; Washington, July 2005, IEEE, Seattle.

Rivas Lopez [a], M.; Sergiyenko, O. & Tyrsa, V. (2008). Machine vision: approaches and limitations, In: *Computer vision,* Xiong Zhihui, (Ed.), pp. 395-428. Editorial: IN-TECH, ISBN 978-953-7619-21-3, Vienna, Austria.

Rivas Lopez [b], M.; Sergiyenko, O.; Aguirre, M.; Devia, L.F.; Tyrsa, V.; & Rendón, I. (2008). Spatial data acquisition by laser scanning for robot or SHM task. *Proceedings of IEEE-IES International Symposium on Industrial Electronics (ISIE-2008)*, p.1458-1463, ISBN 978-1-4244-1666-0, Cambridge, United Kingdom, 30 June -2 July 2008, IEEEXplore, Cambridge.

Rivas Lopez, M.; Sergiyenko, O.; Tyrsa, V.; Hernández Perdomo, W.; Hernández Balbuena, D.; Devia Cruz, L.; Burtseva, L.; & Nieto Hipólito J. I. (2010). Optoelectronic method for structural health monitoring. *International Journal of Structural Health Monitoring*, Vol.9, No.2, March, 2010, SAGE Publications, pp.105-120, ISSN 1475-9217

Rodríguez, J.C., Sergiyenko, O.; Básaca, L.C. (2009). Medición de parámetros biométricos específicos en el rostro humano por medio de barrido láser dinámico (in Spanish). *Proceedings of Congreso Nacional de Estudiantes de Posgrado del Instituto de Ingeniería,* UABC Mexicali B.C, November, 25-27, 2009, 6p., ISBN: 978-607-7753-33-9.

Sergiyenko, O.; Burtseva, L.; Bravo, M.; Rendón, I. & Tyrsa V. (2006). Scanning vision System for Mobile Vehicle Navigation. *Proceedings of IEEE-LEOS Multiconference on Electronics and Photonics (MEP-2006),* p.178-181, ISBN 1-4244-0627-7, Guanajuato, Mexico, 7-10 November, 2006, IEEEXplore, Guanajuato.

Sergiyenko, O.; Tyrsa, V.; Hernandez-Balbuena, D.; Rivas López, M.; Rendón López, I. & Devia Cruz, L.F. (2008). Precise Optical Scanning for practical multiapplications. *Proceedings of IEEE-34th Annual Conference of IEEE Industrial Electronics (IECON'08)*, p.1656-1661, ISBN 978-1-4244-1766-7, Florida, USA, 10-13 November, 2008, IEEEXplore, Orlando.

Sergiyenko, O. [a]; Hernandez, W.; Tyrsa, V.; Devia Cruz, L.; Starostenko, O. & Pena-Cabrera, M. (2009). Remote Sensor for Spatial Measurements by Using Optical Scanning, *Sensors,* 9(7), July, 2009, MDPI, Basel, Switzerland, pp. 5477-5492. ISSN 1424-8220.

Sergiyenko, O. Y. [b]; Tyrsa, V. V.; Devia, L. F.; Hernandez, W.; Starostenko, O. & Rivas Lopez M. (2009). Dynamic Laser Scanning method for Mobile Robot Navigation. *Proceedings of ICROS-SICE International Joint Conference (ICCAS-SICE 2009)*, p. 4884-4889, ISBN: 978-4-907764-33-3, Fukuoka, Japan, August, 18-21, 2009, IEEEXplore, Fukuoka.

Sergiyenko, O. Yu. [c]; Hernandez, W.; Tyrsa, V. V. & Hernández-Balbuena, D. (2009). Precise Optical Scanning for multiuse. *Proceedings of IEEE-35th Annual Conference of IEEE Industrial Electronics (IECON'09)*, pp.3399-3404. ISBN 978-1-4244-4649-0/09, 3-5 November, 2009, Porto, Portugal, IEEEXplore, Porto.

Sergiyenko, O. Yu. (2010) Optoelectronic System for Mobile Robot Navigation. Springer/Allerton Press, Inc., *Journal Optoelectronics, Instrumentation and Data Processing*, Vol. 46, No. 5, October, 2010, pp.414-428 – ISSN 8756-6990

Son, S.; Park, H. & Lee, K. H. (2002). Automated laser scanning system for reverse engineering and inspection. *International Journal of machine tools and manufacture*. Pergamon Press, Great Britain, Vol. 42; No. 8, 2002, p. 889-897, ISSN 0890-6955

Surmann, H.; Lingemann, K.; Nüchter, A.; & Hertzberg, J. (2001). A 3D laser range finder for autonomous mobile robots. *Proceedings of the 32nd ISR (International Symposium on Robotics),* pp. 153 - 158, 19-21 April 2001.

Surmann, H. (2003), An autonomous mobile robot with a 3D laser range finder for 3D exploration and digitalization of indoor environments, *Journal Robotics and Autonomous Systems (JRAS), Elsevier Science*, Volume 45, No. 3-4, December, 2003, pages 181 – 198, ISSN 0921-8890.

Vandapel, N.; Huber, D.F.; Kapuria, A. & Hebert, M. (2004). Natural terrain classification using 3-d ladar data, Proceedings *of IEEE International Conference on Robotics and Automation 2004. IEEE ICRA '04*, Vol. 5, April-May, 2004, 5117–5122, ISSN 1050-4729.

Wallace, R.; Matsuzaki, K.; Goto, Y.; Crisman, J.; Webb, J. & Kanade, T. (1986). Progress in robot road-following, *Proceedings of IEEE International Conference on Robotics and Automation 1986*, Vol. 3, April, 1986, 1615–1621, ISSN 0882-4967.

Wettergreen, D.; Tompkins, P.; Urmson, C.; Wagner, M. & Whittaker, W. (2005) Sun-synchronous robotic exploration: Technical description and field experimentation, *International Journal of Robotics Research*, Vol. 24, No. 1, January, 2005, 3–30, ISSN 0278-3649.

Wijesoma, W.; Kodagoda, K. & Balasuriya, A. (2004). Road-boundary detection and tracking using ladar sensing, *IEEE Transactions on Robotics and Automation*, Vol. 20, No. 3, June, 2004, 456–464, ISSN 1042-296X.

Wulf, O.; Kai, O; Christensen, Henrik I.; Wagner, B (2004), 2D Mapping of Cluttered Indoor Environments by Means of 3D Perception, *International Conference on Robotics & Automation*, ISBN : 0-7803-8232-3, New Orleans, LA, April 2004, IEEE, New Orleans

Wulf, O. & Wagner, B. (2003), Fast 3D Scanning Methods for Laser Measurement Systems, *Proceedings of International Conference on Control Systems and Computer Science*, 2003, p. 312-317, ISBN: 973-8449-18-9 Bucharest, Romania, July 2003.

Wyatt, C.L., (1991). Electro-optical system design: For information Processing .McGraw-Hill, ISBN 0-07-072184-X, New York, 1991, 343p.

Zussman, E.; Schuler, H. & Seliger, G. (1994). Analysis of the geometrical feature detectability constraints for laser-scanner sensor planning. *The International Journal of Advanced Manufacturing Technology*, Vol. 9, No. 1, January, 1994, p. 56–64, ISSN 1433-3015.

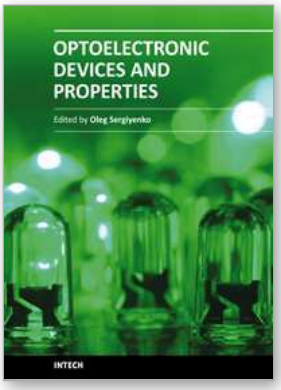

Optoelectronic Devices and Properties

Edited by Prof. Oleg Sergiyenko

ISBN 978-953-307-204-3
Hard cover, 660 pages
Publisher InTech
Published online 19, April, 2011
Published in print edition April, 2011

Optoelectronic devices impact many areas of society, from simple household appliances and multimedia systems to communications, computing, spatial scanning, optical monitoring, 3D measurements and medical instruments. This is the most complete book about optoelectromechanic systems and semiconductor optoelectronic devices; it provides an accessible, well-organized overview of optoelectronic devices and properties that emphasizes basic principles.

How to reference

In order to correctly reference this scholarly work, feel free to copy and paste the following:

Oleg Sergiyenko, Vera Tyrsa, Luís C. Basaca-Preciado, Julio C. Rodríguez-Quiñones, Wilmar Hernández, Juan I. Nieto-Hipólito, Moisés Rivas Lopez and Oleg Starostenko (2011). Electromechanical 3D Optoelectronic Scanners: Resolution Constraints and Possible Ways of Improvement, Optoelectronic Devices and Properties, Prof. Oleg Sergiyenko (Ed.), ISBN: 978-953-307-204-3, InTech, Available from: http://www.intechopen.com/books/optoelectronic-devices-and-properties/electromechanical-3d-optoelectronic-scanners-resolution-constraints-and-possible-ways-of-improvement

INTECH
open science | open minds

InTech Europe
University Campus STeP Ri
Slavka Krautzeka 83/A
51000 Rijeka, Croatia
Phone: +385 (51) 770 447
Fax: +385 (51) 686 166
www.intechopen.com

InTech China
Unit 405, Office Block, Hotel Equatorial Shanghai
No.65, Yan An Road (West), Shanghai, 200040, China
中国上海市延安西路65号上海国际贵都大饭店办公楼405单元
Phone: +86-21-62489820
Fax: +86-21-62489821